Environmental Science
Nano

ROYAL SOCIETY
OF CHEMISTRY
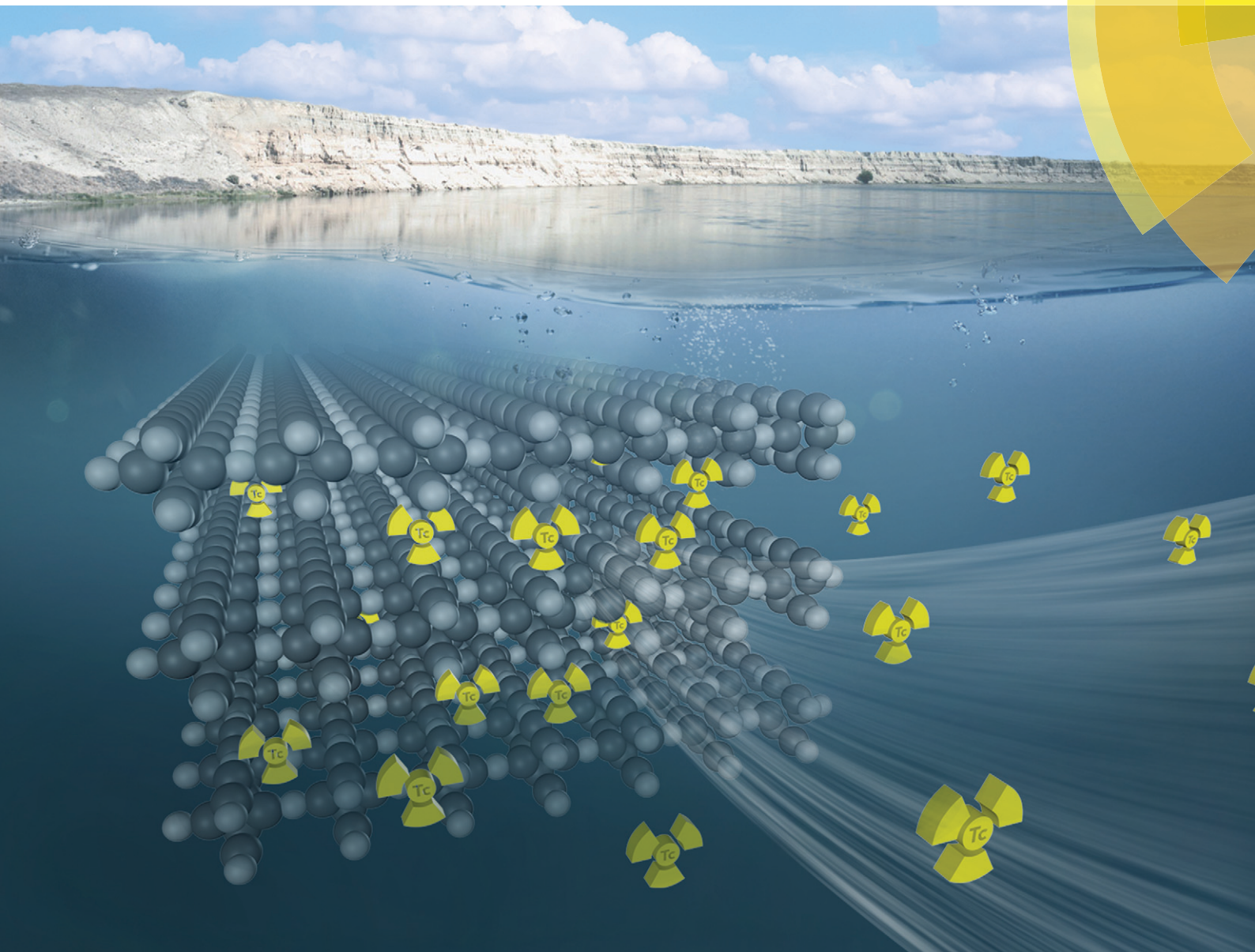
PAPER
Tatiana G. Levitskaia, Sayandev Chatterjee *et al.*
Inorganic tin aluminophosphate nanocomposite for reductive separation
of pertechnetate

175 YEARS

Inorganic tin aluminophosphate nanocomposite for reductive separation of pertechnetate†

Tatiana G. Levitskaia,*[a] Sayandev Chatterjee,*[a] Natasha K. Pence,[a] Jesus Romero,[a] Tamas Varga,[b] Mark H. Engelhard,[b] Yingge Du,[c] Libor Kovarik,[b] Bruce W. Arey,[a] Mark E. Bowden[b] and Eric D. Walter[b]

Pertechnetate (TcO_4^-) is the most abundant chemical form of the radioactive contaminant ^{99}Tc present in legacy nuclear waste streams and in the subsurface of nuclear waste storage sites. One proposed remediation approach is reductive separation of TcO_4^- and sequestration in low-temperature waste forms. The development of relevant technologies has been slow due to the lack of reductive materials that retain their functionality and are otherwise suitable for application in multicomponent and aggressive media such as highly alkaline, brine-like solutions typifying nuclear tank wastes. In this work, a tin-based reductive material was prepared, and its potential utility for the separation of TcO_4^- from alkaline nuclear wastes was demonstrated. This material consists of Sn(II/IV) phosphate supported by a polycrystalline aluminophosphate matrix. The aluminophosphate matrix is inert to the reaction conditions and offers the benefits of high stability and low solubility in concentrated alkaline solutions. This Sn(II/IV)-based material exhibits a high loading capacity for Tc and selectively removes a major fraction of TcO_4^- from the tank waste supernatant simulant, which contains 7.8 M total sodium and 2.43 M free hydroxide concentrations. Observed K_d values for Tc are about 13 000 and 2200 mL g^{-1} for simulant solutions containing no or 33 mM Cr(VI), respectively, positioning Sn(II/IV) aluminophosphate among the best-performing reductive sorbents for TcO_4^- developed to date. This advanced behaviour is attributed to the synergistic combination of the Sn(II/IV) aluminophosphate functionalities. The presence of Sn(II/IV)-rich fibres facilitates the reduction of TcO_4^- to Tc(IV), which is embedded along the fibre branches. Importantly, the Sn(IV)-containing inert polycrystalline matrix also incorporates Tc(IV) which triggers its crystallization to cassiterite SnO_2 phase and stabilizes Tc(IV) in the polycrystalline matrix.

Nano impact

Tc-99 is a radioactive contaminant of significant environmental concern. The total Tc inventory continues to increase worldwide due to generation of nuclear power, and methods are needed for its separation from multi-component matrices and stabilization for long-term storage. In order to address this need, we describe a novel redox active Sn(II/IV) aluminophosphate nanocomposite that can reductively separate TcO_4^-, the most common chemical form of Tc, converting it to less mobile Tc(IV) and providing a robust platform for potential immobilization.

Introduction

Technetium-99 (Tc), a high-yield fission product of uranium-235 and plutonium-239, has been generated in significant

[a] *Energy and Environment Directorate, Pacific Northwest National Laboratory, Richland, WA 99354, USA. E-mail: Tatiana.Levitskaia@pnnl.gov, Sayandev.Chatterjee@pnnl.gov*
[b] *Environmental and Molecular Sciences Laboratory, Pacific Northwest National Laboratory, Richland, WA 99354, USA*
[c] *Physical and Computational Sciences Directorate, Pacific Northwest National Laboratory, Richland, WA 99354, USA*
† Electronic supplementary information (ESI) available: Complementary characterization results for the Sn–Al–PO$_4$ composite before and after loading with TcO_4^- including figures of the IR spectra, X-ray diffraction and elemental maps through EDS. See DOI: 10.1039/c6en00130k

quantities by nuclear weapon production during the Cold War.[1] The total Tc inventory continues to increase worldwide due to the generation of nuclear power, driving interest to advance the understanding of Tc chemistry and to reduce the uncertainty associated with its long-term environmental impact. Because of its long half-life (213 000 years),[2] Tc contributes significantly to the radiotoxicity of nuclear wastes (representative examples being the U.S. Department of Energy (DOE) Hanford and Savannah River Sites) and affects waste processing and remedial decisions. It exists predominantly in the liquid fractions of alkaline tank waste, generally in the anionic form of pertechnetate, TcO_4^-. The high aqueous solubility of TcO_4^- coupled with its weak retention in soils and minerals results in its mobile behaviour in the subsurface,[3]

making immobilization of TcO_4^- in cementitious or mineral waste forms for long-term storage difficult. Reductive separation of TcO_4^- and the resulting sequestration of the much less soluble Tc(IV) product is a commonly considered remediation strategy. Despite extensive past investigations of the Tc(VII)/Tc(IV) couple in presence of different reducing systems such as zero valent iron,[4] Fe(II)/goethite,[5] magnetite,[6] Fe(II)-bearing oxides,[7] and sulfides,[8,9] limited progress has been achieved in developing reductive materials for practical separation and sequestration of TcO_4^- from solutions high in ionic strength and alkalinity typifying nuclear waste matrices.

Divalent tin, Sn(II), is known for its strong reductive character, and $SnCl_2$ is widely used for reduction of $^{99m}TcO_4^-$ in physiological buffer media during the preparation of ^{99m}Tc-labeled radiopharmaceuticals.[10] Similarly, $SnCl_2$ has demonstrated quantitative reduction of TcO_4^- and precipitation of the resulting insoluble Tc(IV) at high pH.[11] A recent systematic investigation of the Tc(VII)/Tc(IV) couple in chloride solutions of variable concentration concluded that $SnCl_2$ is an effective reductant for TcO_4^- and completely converts it to Tc(IV), even at high ionic strengths and a pH of 14.5.[12] However, the applicability of $SnCl_2$ for separation purposes is limited because of its relatively high aqueous solubility, and the requirement of an additional step for the removal of the reduced Tc(IV).

In an effort to combine reductive and sorptive functionalities in one material, Sn(II) apatite $Sn_5(PO_4)_3$(F, Cl, OH) was designed,[13] albeit through a complicated synthetic pathway. This material demonstrated quantitative removal of Tc from dilute solutions, even outperforming $SnCl_2$; however, its effectiveness was significantly reduced in the alkaline brine-like solution simulating nuclear waste, the diminished effectiveness attributed to the presence of Cr(VI) interfering with the reduction of Tc(VII) by Sn(II).[14] A similar approach has been explored using a nanoporous stannous phosphate material, which was shown to effectively reduce and sequester not only TcO_4^- but also other redox-sensitive contaminants including Np(V), Th(IV), and Cr(VI) from dilute bicarbonate media.[15] While this material is promising, it lacks selectivity for TcO_4^-, which might disqualify it for application in the complex media that characterize tank waste supernatants.

In an effort to address the practical drawbacks of Sn-based materials while preserving their promising qualities, the objective of this work was to develop a Sn-containing composite material offering the synergistic benefits of reductive uptake of TcO_4^- from a complex, alkaline, high ionic strength matrix and selective association of reduced Tc(IV) with the material. It is well established that any precipitated Tc(IV) deposited on surfaces free to the atmosphere is highly susceptible to reoxidation back to the mobile TcO_4^- state.[16,17] A way to prevent the reoxidation of Tc(IV) is to increase its oxidation potential either through a strong chemical association of Tc(IV) with the sorbent material or by incorporating it as a thermodynamically stable phase integral to the sorbent matrix, such that it is more resistant to oxidation compared to free Tc(IV). Recent work has demonstrated that Tc(IV) obtained

from reduction of TcO_4^- by goethite-based Fe(II) in solution and subsequently incorporated in the octahedral site of goethite by substituting Tc(IV) for Fe(III) is resistant to reoxidation when exposed to oxidizing conditions.[5] We hypothesize that a composite system containing mixed Sn-containing phases benefits from a two-in-one functionality, where Sn(II) serves as a reductant for TcO_4^- while the presence of an inert crystalline platform serves to integrate Tc(IV) within any structurally compatible phases. Bearing in mind the octahedral nature of Tc(IV) oxide, the presence of any Sn phases possessing high complementarity for Tc(IV) can be uniquely advantageous.

One such phase is cassiterite, SnO_2 with a rutile structure; literature data suggest that it is possible for Tc(IV) dioxides to (a) adapt a cassiterite structure as observed in the case of TcO_2 (ref. 18) or (b) be incorporated within a rutile structural framework as observed with TiO_2.[19] In this work, to obtain a sorbent framework suitable for the separation of the sequestered Tc(IV), Sn(II)/(IV) is combined with an aluminophosphate supporting matrix. The selection of this matrix is based on recent studies demonstrating that incorporation of substantial quantities of both Sn(II) and Sn(IV) within the aluminophosphate framework can be achieved (ref. 20 and the references therein). Additional considerations supporting this choice are the high stability and low solubility of the aluminophosphate phase in concentrated alkaline solutions as well as its lack of interfering redox activity. The obtained Sn(II)/(IV) aluminophosphate-supported composite (referred to in the text as **Sn–Al–PO$_4$**) was structurally characterized before and after reductive uptake of TcO_4^-, and its selectivity over interfering redox species, most notably Cr(VI), was evaluated using a multicomponent, brine-like, highly alkaline solution.

Experimental

Chemicals and materials

Radiation safety disclaimer! *Technetium-99 has a half-life of 2.12×10^5 years and emits a low-energy (0.292 MeV) β particle; common laboratory materials provide adequate shielding. Normal radiation safety procedures must be used at all times to prevent contamination.*

$SnCl_2 \cdot 2H_2O$ was purchased from JT Baker. All other chemicals (reagent grade) were purchased from Sigma Aldrich or Baker & Adamson Chemicals and used without further purification. Deionized (DI) water was used for the preparation of the aqueous solutions. NH_4TcO_4 was obtained from in-house stocks available at the Radiochemical Processing Laboratory at Pacific Northwest National Laboratory, WA, USA.

Solution preparation. The affinity of the **Sn–Al–PO$_4$** composite towards TcO_4^- and the kinetics of its uptake initially were evaluated from stock solutions prepared by dissolving NH_4TcO_4 in an aqueous solution composed of 2 M NaOH and 2 M $NaNO_3$. As the composite exhibited favourable uptake of TcO_4^- from these media, uptake kinetics was further

monitored from a TcO_4^--containing Hanford low activity waste (LAW) simulant solution. This simulant was developed based on component concentrations designed to match the output of Hanford Tank Waste Operation Simulator (HTWOS) model runs used previously in support of the River Protection Project System Plan Revision 6 (ref. 21) according to a protocol reported elsewhere.[22] The simulant composition is listed in Table 1. In order to explore the influence of Cr(VI) on TcO_4^- uptake, an alternate version of the same simulant was also prepared where chromate was excluded from the simulant composition.

Sn–Al–PO4 composite synthesis. In a general procedure, 0.38 g (1.01 mmol) of $Al(NO_3)_3 \cdot 9H_2O$ and 1.48 g (12.34 mmol) of $NaH_2PO_4 \cdot 7H_2O$ were dissolved in ~50 mL of deionized water. The solution was stirred for about 15 minutes followed by the addition of 0.68 g of $SnCl_2 \cdot 2H_2O$ (3.02 mmol) and 0.26 g of $SnCl_4 \cdot 5H_2O$ (0.75 mmol). To the resultant suspension, 0.5 M NaOH solution was added with stirring until a pH of 12.0 was achieved. It is to be noted that the composite chemistry is highly dependent on the pH of the reaction solution and the reaction conditions. Consequently, we observed some variability in the composite and the better performing specimens are reported here. The mixture was transferred to a Teflon-lined autoclave and kept at 140 ± 5 °C for 72 hours to yield the aggregate. The obtained off-white solid was gravity-filtered, washed with excess water until neutral pH of the rinse was achieved, and dried. The elemental analyses of the samples were obtained from electron dispersive spectrometry (EDS) data and are summarized in a later section and in Table 2.

Batch contact experiments. The Sn–Al–PO4 composite (25 mg) was suspended in 5 mL of a ~20 μM (~2.1 ppm) NH_4TcO_4 solution in 2 M NaOH/2 M $NaNO_3$ so that the ratio of the solution volume to the weight of the sorbent was 200 mL g^{-1}, agitated using a rotor shaker, and the liquid phase was periodically aliquoted after centrifugation (2000 rpm for 15 minutes) for analysis of ^{99}Tc uptake. The batch contacts using LAW simulants were conducted by combining 25 mg of the composite and 25 mL of ~40 μM NH_4TcO_4 solution in the LAW simulant (solution-to-sorbent ratio is 1000 mL g^{-1}).

Table 1 Composition of the LAW simulant

Waste constituent	Average concentration, mol L^{-1}
Al	0.48
K	0.06
Na	7.80
Cl$^-$	0.06
CO_3^{2-}	0.43
F$^-$	0.05
NO_2^-	0.88
NO_3^-	2.53
PO_4^{3-}	0.08
SO_4^{2-}	0.13
TOC total	0.12
Free OH$^-$	2.43
Cd	0.00025
Cr	0.033
Pb	0.0004

Table 2 Elemental analysis of the marked regions in Fig. 3 for the untreated composite obtained from EDS analyses showing the respective atomic percentages of the elements

Region	Atomic percent, %					
	C	O	Na	Al	P	Sn
1	20.2	52.6	1.4	2.5	9.4	13.9
2	16.3	56.4	1.6	2.5	10.3	12.9
3	11.3	70.5	0.95	0.68	8.2	8.3
4	12.6	69.5	1.9	0.42	7.2	8.3

Two types of LAW simulant solutions, containing either 0 or 33 mM Cr(VI), were tested. The kinetics of TcO_4^- uptake was monitored for 24 and 72 hours from 2 M NaOH/2 M $NaNO_3$ and simulant solutions, respectively. At different time points post beginning of the experiment, batch contact samples were centrifuged, and 20 μL of the contact solution was removed for analysis. The concentration of TcO_4^- in the sub-samples was quantified by liquid scintillation counting (LSC). For each time point, the solution volume was corrected for the withdrawn aliquot. The distribution coefficient, K_d (mL g^{-1}), was calculated using eqn (1),

$$K_d = \frac{C_i - C_t}{C_t} \times \frac{V}{W_C} \qquad (1)$$

where C_i is the initial concentration of pertechnetate in the contact solution, C_t is the Tc concentration of Tc in the solution at time t, V is the volume of the contact solution in milliliters, and W_C is the weight of the dry composite material in grams.

Characterization techniques. The structural and morphological features of the composite materials before and after exposure to TcO_4^- solution in DI water were examined by X-ray diffraction (XRD), scanning electron microscopy (SEM)/ energy dispersive spectroscopy (EDS), and transmission electron microscopy (TEM) studies, while the vibrational structure of the composites were evaluated by infrared (IR) spectroscopy. Changes in the metal center chemical environment upon Tc uptake and the Tc oxidation state in the composite matrix were monitored through X-ray photoelectron spectroscopy (XPS), *in situ* TEM, and electron paramagnetic resonance (EPR) studies. To prepare Tc-loaded samples for diffraction, microscopy and spectroscopic studies, ~50 mg of the composite material was brought into contact with 1 mL of the 10 mM TcO_4^- solution in DI water under agitation at room temperature. After 24 hours the liquid phase was removed from the sample by centrifugation and decantation, and the loaded composite was rinsed with DI water (5 × 10 mL) and air-dried at room temperature until completely dry. LSC analysis indicated nearly quantitative uptake of Tc by the composite so that the Tc loading of the Sn–Al–PO4 composite was estimated to be 0.2 mmol g^{-1} or 20 mg g^{-1}.

FTIR measurements were conducted using a spectrometer (ALPHA model, Bruker Optics) operated with OPUS software (Version 6.5, Build 6.5.92). Samples were run directly on a diamond attenuated total reflectance (ATR) cell. For each
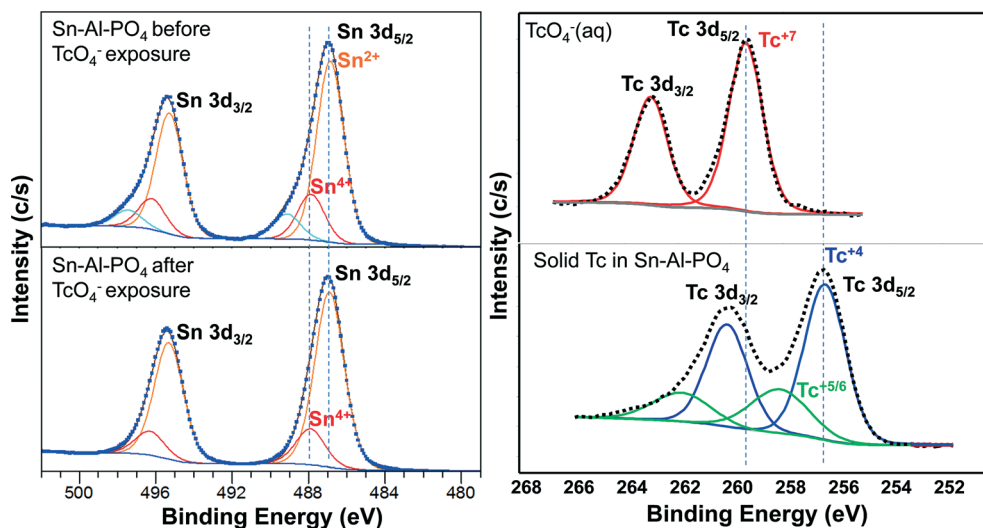
Fig. 1 (Left) Overlays of X-ray photoelectron spectra of Sn $3d_{5/2}$ and $3d_{3/2}$ regions of the **Sn–Al–PO₄** composite (top) before and (bottom) after exposure to 10 mM TcO_4^-; (blue squares = experimental data; orange trace = Sn(II) fit based on the literature; red trace = Sn(IV) fit based on the literature[31,32]). (Right) X-ray photoelectron spectrum of (top) Tc $3d_{5/2}$ and $3d_{3/2}$ regions of pure NH_4TcO_4 stock and (bottom) Tc region in the composite after being exposed to TcO_4^- for 24 hours (black dashed line = experimental data; red trace = TcO_4^- fit based on the literature;[33,34] dark blue trace = Tc(IV) fit based on the literature;[33,34] green trace = Tc(V/VI) fit based on the literature[33,34]).

sample, 24 scans with a resolution of 4 wavenumbers (cm^{-1}) were averaged to give the final spectrum. A background of ambient air was used for all samples.

XRD patterns of the samples were recorded on a Rigaku Miniflex 600 Bragg–Brentano diffractometer equipped with a fixed Cu anode operating at 40 kV and 15 mA. XRD patterns were collected in the 5–100° 2θ-range with 0.02° steps at a rate of 4 s per step. The powders were packed in well in a zero-background plate held within a custom holder with Kapton X-ray windows to prevent spread of radioactive contamination. Phase identification was performed using JADE 9.5.1 from Materials Data Inc. and the 2012 PDF4+ database from ICSD.

XPS was used to identify the oxidation states associated with the solid composites before and after TcO_4^- uptake. Spectra were recorded using a Kratos AXIS Ultra DLD system equipped with a monochromatic Al Kα X-ray source (1486.7 eV) and a hemispherical analyzer. Samples were mounted using double-sided Scotch brand tape attached to a silicon substrate. The instrument work function was calibrated to give a binding energy (BE) of 83.96 ± 0.1 eV for the Au $4f_{7/2}$ line for metallic gold and the spectrometer dispersion was adjusted to give a BE of 932.62 ± 0.1 eV for the Cu $2p_{3/2}$ line of metallic copper. High resolution analyses were carried out with an analysis area of 300 × 700 microns using a pass energy of 40 eV with a step size of 0.1 eV. Surface charge was eliminated using a charge neutralizer and data were corrected through referencing the 285.0 eV C 1s peak. The percentages of individual elements detected were determined from the relative composition analysis of the peak areas of the bands on the basis of the relative peak areas and their corresponding sensitivity factors to provide relative compositions. XPS peak fitting was performed using CasaXPS.

SEM analysis was performed using an FEI Quanta 3DFEG Dual Beam microscope operated at 10–20 kV. The samples were prepared by two independent methods; in the first method, the sample particles were dispersed onto carbon tape and coated with ~5 nm of carbon to minimize charge effects. In the second method, samples were mounted on the tape and polished using typical metallographic techniques to avoid colloidal silica from polishing. Compositional analysis was performed using an Oxford 80 mm^2 SDD EDS detector. For quantitative EDS analysis, calculated K factors provided by INCA software were used. No correction for absorption within the specimen was performed. Both secondary electron images (SE) and backscatter electron images (BSE) were recorded.

For TEM analyses separate instruments were used for non-radiological samples and radiological (Tc loaded) samples for ease of operation. The samples free of Tc were analyzed on an FEI Titan 80–300 kV transmission electron microscope operated at 300 kV. The microscope is equipped with a CEOS aberration corrector for the probe-forming lens, which allows imaging in scanning mode with sub-ångstrom resolution. Images were acquired on a high angle annular dark field (HAADF) detector. The detection angle was kept 3 times higher than the probe convergence angle of 18 mrad. Compositional analysis was performed with an EDAX Si(Li) EDS detector. Post-acquisition quantification and evaluation of the spectra were performed using the FEI TIA software package. The samples containing Tc were analyzed using an aberration corrected scanning transmission electron microscope (STEM) (JEOL JEM-ARM200F) operated at 200 kV. The images were acquired on a HAADF detector with a beam convergence of 27.5 mrad. Elemental analysis was performed using EDS using high collection angle SSD.
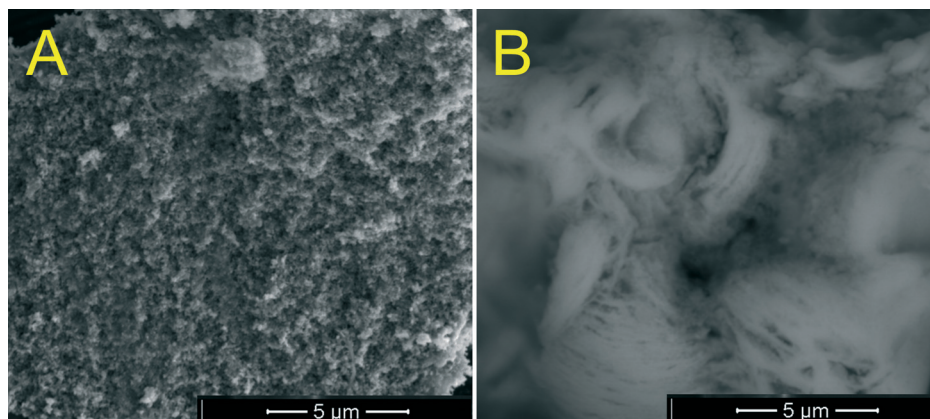
Fig. 2 Representative SEM images of the **Sn–Al–PO₄** composite (A) before and (B) after exposure to TcO₄⁻.

STEM–EDS data were processed using Analysis Station (version 3.8.0.52, JEOL Engineering, Co., Ltd.).

EPR spectra were acquired on a Bruker EMX spectrometer equipped with an ER4102ST resonator (spectra at room temperature and 120 K) or an ER4116DM Dual Mode resonator (spectra at 5 K) and an Oxford ESR910 cryostat. Tc-containing radiological samples were doubly contained by employing unbreakable FEP tube liners (Wilmad) inside traditional quartz EPR tubes. The sample configurations used 3.15 mm inner diameter liners and 5 mm outer diameter tubes.

Results and discussion

Characterisation of the Sn–Al–PO₄ composite before TcO₄⁻ uptake

The IR spectrum of the solid **Sn–Al–PO₄** composite showed strong bands at ~1065 and ~980 cm⁻¹,[23] which are consistent with the symmetric and asymmetric Sn–O–P stretching vibrations, respectively,[24] suggesting the presence of a mesoporous Sn-based phosphate framework (Fig. S1†).[25] A broad asymmetric band at *ca.* 3440 cm⁻¹ is due to the ν_{O-H} stretching vibration of hydrogen-bonded geminal OH groups and water molecules, and that at 1634 cm⁻¹ corresponds to the bending of water.[26] A similar band was observed by Huang and co-workers for nanolayered, 15 Å, tin phosphate materials, and indicates the presence of interlayer water molecules,[27] suggesting the existence of a layered structure in our **Sn–Al–PO₄** composite. The band at 540 cm⁻¹ is consistent with O–P–O bending vibrations that are characteristic of AlPO₄.[28,29]

The X-ray diffractogram of the **Sn–Al–PO₄** composite indicates the poor crystallinity of this material (Fig. S2†). Only the SnO₂ (cassiterite) phase could be identified with any certainty, although there are clearly additional diffraction peaks present.[30] These peaks could in part be attributed to an AlPO₄ phase,[30] suggesting that the actual composition could be a combination of these phases. However, the poorly defined diffraction profile did not allow positive identification.

Photoelectron spectroscopy was used to confirm the oxidation states associated with the Sn centres. The Sn region of the

photoelectron spectrum of **Sn–Al–PO₄** before TcO₄⁻ exposure can be fit by two sets of doublets (Fig. 1). The two low binding energy peaks (3d₅/₂) are centred at 486.9 eV and 487.9 eV and can be attributed to Sn(II) and Sn(IV), respectively.[31,32] The intensities of the Sn(IV) peaks are significantly lower than those of Sn(II), indicating the surface of the composite to be primarily dominated by tin in the Sn²⁺ oxidation state. There is an additional low intensity doublet with a 3d₅/₂ value of 489.1 eV, suggesting the presence of another high oxidation state chemical form of Sn in the composite. While XRD did not give a clear indication of any Sn(II) containing phases, XPS suggests it to be the dominant oxidation state in the material.

Representative SEM images (Fig. 2A) of the composite illustrate a highly amorphous material indicating a large surface area for uptake. A closer inspection of the materials through TEM (Fig. 3) indicates two distinct morphological features within the materials, the general material being characterized by an amorphous matrix impregnated with small islets of crystalline fibers. The amorphous matrix exhibits a highly diffused diffraction and is largely characterized by small two-dimensional lamellar particles, ranging from 30 to 60 nm in edge length. The EDS (Table 2) of the polycrystalline matrix shows the dominance of Sn, associated with a lower quantity of Al. There is a significant amount of P, presumably present as PO₄³⁻. The Sn:Al:P molar ratio in the polycrystalline matrix is 1:0.18:0.73. This is consistent with the Sn:Al molar ratio of 1:0.22 used in the preparation of the material, indicating that nearly all Al used in the synthesis comprises the polycrystalline matrix. The crystalline fibers are characterized by an aggregation of linear wires, each ranging from ~0.6 to 1 μm in length, and display a structured diffraction pattern with *d* spacing of 6.89 Å. The diffraction data do not match with any of the currently known Sn and/or Al phosphates in the crystal structure database, and further characterization of this phase is a focus of future work. The EDS analysis of the crystalline fibers shows that they are primarily composed of Sn and phosphate with a negligible quantity of Al, the Sn:Al:P ratio being 1:0.06:0.92.

The EPR spectrum of the powdered off-white composite shows no resonances at room temperature. Taken together,

This journal is © The Royal Society of Chemistry 2016

Environ. Sci.: Nano, 2016, **3**, 1003–1013 | **1007**
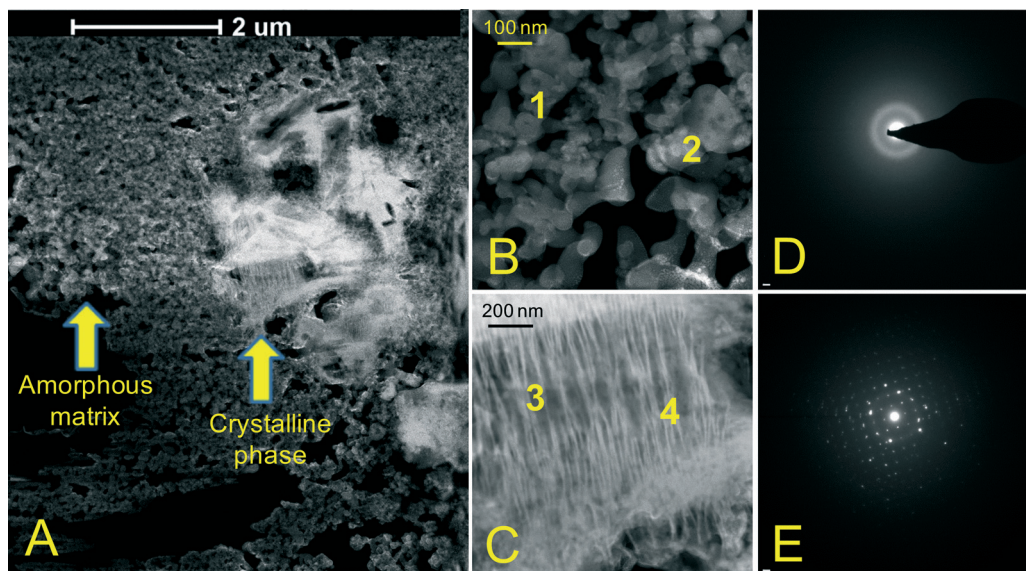
Fig. 3 Representative TEM images of the **Sn–Al–PO₄** composite: (A) overall representation, (B) polycrystalline matrix, (C) crystalline fibers, (D) diffraction of polycrystalline matrix, (E) diffraction of crystalline fibers.

these results suggest that the **Sn–Al–PO₄** composite consists of a multi-component layered, microporous matrix containing a mixture of Sn(ɪɪ) and Sn(ɪᴠ) doped with Al, onto which highly crystalline fibers rich in Sn and phosphate are embedded.

Characterization of the Tc-loaded Sn–Al–PO₄ composite

The IR spectrum of the TcO_4^--loaded **Sn–Al–PO₄** sample is similar to that of the untreated sample showing strong bands corresponding to the symmetric and asymmetric Sn–O–P stretching vibrations[24] at ~1065 and ~980 cm^{-1} (ref. 23), respectively, as well as the broad asymmetric ν_{O-H} stretching vibration at *ca.* 3440 cm^{-1} (Fig. S1†). Two noticeable differences in these spectra are (i) the appearance of a new band at 1435 cm^{-1}, in addition to the interlayer water bending band at 1634 cm^{-1}, and (ii) the splitting of the sharp single band at 550 cm^{-1} into multiple bands.

While no significant differences are observed in the XRD profile of the **Sn–Al–PO₄** composite prior and post loading with TcO_4^-, small changes are seen, which resemble "erosion" of some and evolution of other phases (Fig. S2†). SnO_2 is still the dominant phase,[30] while the other phases that were observed in the untreated composites, are still present. The phases are observed to have smaller crystallite sizes.

X-ray photoelectron spectroscopy measurements demonstrated that a sufficient quantity of Tc was incorporated into **Sn–Al–PO₄** to allow quantification of its uptake (Fig. 1 with an estimated 47 mg incorporation of Tc per gram of composite. The Sn 3d region of the photoelectron spectrum of the Tc-loaded **Sn–Al–PO₄** composite shows no prominent changes in the respective intensities of the Sn^{2+} and Sn^{4+} bands in comparison with unexposed material. This is to be expected because the small fraction of Sn(ɪɪ) that can be oxidized to

Sn(ɪᴠ) by Tc(ᴠɪɪ) is insignificant compared to the overall Sn concentration. It is worth noting that the low intensity doublet with a 3d$_{5/2}$ value of 489.1 eV corresponding to an additional Sn(ɪᴠ) species does not appear in the Tc-loaded composite. This result is consistent with the transformation of the Sn(ɪᴠ) phases and enhancement of the cassiterite fraction upon Tc exposure demonstrated by the XRD and TEM measurements. While the exact origin of this Sn species is still under investigation, the fact that the exposure to TcO_4^- and its reductive uptake results in the consumption of a Sn species with a higher oxidation state is consistent with the TcO_4^- uptake by the composite not being a simple redox process but involving a more complex pathway. No noticeable changes are observed in the Al or P regions of the photoelectron spectra in going from the unloaded to the Tc-loaded sample.

A photoelectron spectrum of the solid NH_4TcO_4 salt was collected to serve as a Tc(ᴠɪɪ) reference. The Tc 3d spectrum can be fit by a single doublet with a lower binding energy peak at 259.4 eV corresponding to 3d$_{5/2}$. This value is in a good agreement with the NIST standard for Tc(ᴠɪɪ) at 259 eV.[32,33] The Tc 3d spectrum of the **Sn–Al–PO₄** composite exposed to TcO_4^- exhibited a profile drastically different from that of the Tc(ᴠɪɪ) reference. There are now two sets of doublets with lower binding energies centred at 255.9 eV and 258.2 eV, suggesting a reductive sorption that involves a complete reduction of TcO_4^-. The doublet with 3d$_{5/2}$ binding energy at 255.9 eV can be assigned to Tc(ɪᴠ) species,[33] and the second doublet with 3d$_{5/2}$ binding energy at 258.2 eV could arise from a species with an intermediate Tc(ᴠ)/Tc(ᴠɪ) oxidation state as it is positioned between the reported binding energy ranges for Tc(ᴠɪɪ) (259.5–259.9 eV) and Tc(ɪᴠ) (256.6–257.6 eV) species.[33,34] The absence of adequate XPS spectral literature data on Tc(ᴠɪ) or Tc(ᴠ) oxides or oxyanions precludes

1008 | *Environ. Sci.: Nano*, 2016, **3**, 1003–1013

This journal is © The Royal Society of Chemistry 2016

assignment of the exact oxidation state associated with this species. Overall, the generation of Tc as predominantly Tc(ɪᴠ) along with minor Tc(ᴠ/ᴠɪ) species, coupled with complete absence of Tc(ᴠɪɪ), does indicate the complete reduction of the sorbed TcO_4^-. It is significant that the spectrum of the exact same sample of **Sn–Al–PO₄** composite exposed to TcO_4^-, taken six months after the exposure, still exhibits the Tc(ɪᴠ) signal (lower binding energy ~256 eV) with no appearance of a Tc(ᴠɪɪ) band, suggesting the resistance of the species towards reoxidation to TcO_4^-. This enhanced stability of the Tc(ɪᴠ) species is an important observation, as free Tc(ɪᴠ) is usually susceptible to oxidation to TcO_4^- under oxic conditions. It is also important to note that there is a significant loss in Tc photoelectron intensity, which might suggest the Tc migrating from the surface into the sample core.

Representative SEM images (Fig. 2B) of the TcO_4^--loaded **Sn–Al–PO₄** composite illustrates little islets of aggregation of the crystalline fibers embedded within the matrix. A closer inspection of the exposed composite through TEM (Fig. 4) demonstrates changes in both the matrix and the fibers. Interestingly, representative TEM images of the matrix, which exhibited an amorphous character for the unexposed composite, show the formation of a new, cake-like structure. The selected area electron diffraction (SAED) of the matrix reveals a highly structured diffraction with well-defined *d*-spacings, indicating an enhancement of crystallinity of the matrix upon uptake of Tc (Fig. 4F). The diffraction pattern can now be accurately fit to a cassiterite SnO_2 crystal structure. However, the cassiterite phase is not the only phase present in the matrix, as EDS (Table 3) shows a significant amount of P and Al, suggesting that either some amorphous or polycrystalline phase associated with these elements are present in the matrix, or that the crystallinity of aluminophosphate also increases similarly to the cassiterite phase. Based on the appearance of the polycrystalline pattern in the diffractogram, the former seems to be more likely. The matrix is observed to uptake Tc in the bulk, the Sn : Al : Tc ratio in the matrix being

1 : 0.15 : 0.05, indicating 5% Tc loading with respect to Sn (the elemental mapping of the key elements other than Tc is shown in the ESI,† Fig. S3). Therefore, the TEM analysis suggests that the formation of cassiterite phase is facilitated by TcO_4^- exposure as it is not as dominant in the untreated composite. The fact that this change is not picked up by bulk diffraction technique is due to the fact that the amount of TcO_4^- is small compared to the overall amount of the bulk sample for the change to be discernible in the bulk material. Also, treatment of the composite with DI water results in no such enhancement in the cassiterite phase, suggesting that it is generated upon Tc exposure. This is a significant result suggesting the generation of the cassiterite phase to be the result of the interaction of the composite with Tc and points to a strong Tc(ɪᴠ) association with the matrix and a possible Tc(ɪᴠ) incorporation into the cassiterite phase.

Following pertechnetate contact, the crystalline Sn phosphate fibers show formation of uneven deposits along the lengths of the fibers, and deposits seem to glue the fibers together (Fig. 4C). EDS analysis of these deposits shows a predominance of Tc, indicating the immobilization of Tc onto these fibers with the Sn : Al : Tc ratio of 1 : 0.05 : 0.20 or 20% Tc loading with respect to Sn (Table 3; the elemental mapping of the key elements other than Tc is shown in supporting information, Fig. S4†). The SAED pattern of the fibers (Fig. 4G) indicates that the fibers retain their crystallinity upon Tc uptake, though the diffraction is somewhat diffused compared to the unexposed composite.

The EPR spectrum (Fig. 5A) of the TcO_4^--loaded **Sn–Al–PO₄** composite shows no resonances at room temperature. On lowering the temperature to 125 K, a broad new spectrum appears with faint hyperfine resonances corresponding to two sets of equally spaced 10 hyperfine resonances (Fig. 5B); this is suggestive of two different chemical environments, each with a nuclear spin of 9/2. This corresponds to paramagnetic Tc species, and the broad nature of the spectrum with faint hyperfine features is consistent with a Tc(ɪᴠ) species. A
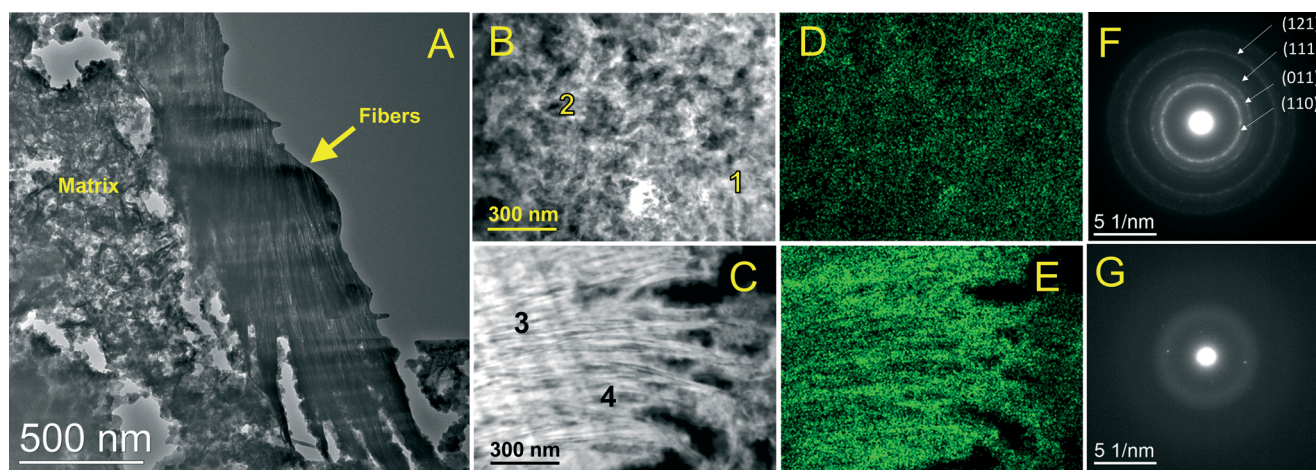
Fig. 4 Representative TEM images of the Tc-loaded **Sn–Al–PO₄** composite. (A) Broader overview showing both the composite matrix and the Sn(ɪɪ/ɪᴠ) fibers; (B, C) respective magnified images of the matrix and the fibers; (D, E) Tc elemental mapping of the matrix and the fibers; (F) SAED of the matrix; and (G) SAED of the fibers.

Table 3 Elemental analysis of the marked regions in Fig. 4 for the Tc-loaded **Sn–Al–PO$_4$** obtained from EDS analyses showing the respective atomic percentages of the elements

Region	Atomic percent, %						
	C	O	Na	Al	P	Tc	Sn
1	16.4	56.3	1.3	2.3	10.6	0.13	12.9
2	17.3	56.4	1.4	1.7	10.3	0.02	12.9
3	12.5	69.3	0.96	0.19	7.3	2.0	7.7
4	12.9	70.2	0.96	0.49	7.0	1.0	7.4

further temperature decrease to 2.5 K significantly increases signal intensity while preserving band energy and hyperfine profile (Fig. 5A and S5†). Further, faint hyperfine lines are observed in the low field section (more evident in the first derivative spectrum as shown in Fig. S5A†) which confirms the formation of Tc(IV). These lines are attributed to zero field splitting which is possible with a 3/2 spin of Tc(IV) and not in an $S = 1/2$ system such as Tc(VI). While observation of Tc(IV) spectra at temperatures higher than 6 K is rare, a prominent Tc(IV) EPR spectrum with resolved hyperfine profile has been reported for polycrystalline K$_2$[TcF$_6$]–K$_2$[PtF$_6$] mixed crystals at 77 K, which transformed into the broad unresolved signal at room temperature.[35]

Overall the observed Tc(IV) spectrum is different from that exhibited by Tc(IV) species incorporated within SnO$_2$ rutile single crystals.[36] However, the faint hyperfine profile observed in the low field section resembles that of Tc(IV) in the SnO$_2$ rutile based on the comparison of the derivatives of our experimental 2.5 K spectrum and of the spectrum simulated using the parameters reported Tc(IV) in the SnO$_2$ cassiterite (Fig. S5B†).[36] The difference between these spectra is attributed to the dissimilar chemical nature of the **Sn–Al–PO$_4$** composite and pure SnO$_2$ as well as dissimilar experimental protocols for the incorporation of Tc(IV) in these materials resulting in different Tc(IV) products. What is of significant importance is that EPR indicates the presence of two Tc(IV) chemical environments, both are different from chemically

pure TcO$_2$·xH$_2$O,[37] presumably due to the two different modes of incorporation of Tc(IV) into the composite. This is consistent with the SEM/EDS and TEM results, which show the presence of Tc both in the crystalline fibers and in the bulk matrix. Further, the observation of a Tc(IV) spectrum at temperatures higher than 2.5 K is suggestive of a slower relaxation that can point to these Tc(IV) species having a lower symmetry than symmetric Tc(IV) species such as pure TcO$_2$·xH$_2$O.[37]

Taken together, the diffraction, photoelectron spectroscopy, microscopy and EPR spectroscopy results reveal the ability of the **Sn–Al–PO$_4$** composite to uptake and reduce TcO$_4^-$ and to incorporate generated Tc(IV) into two different phases. It was concluded that surface precipitation of Tc(IV) plays only a minor role in this mechanism as no reoxidation of Tc(IV) to Tc(VII) was observed by XPS after storing the Tc-loaded **Sn–Al–PO$_4$** composite for 6 months under ambient aerated conditions. The strong affinity of Sn- and P-rich fibers toward TcO$_4^-$ is driven by the redox reaction of Sn(II) with Tc(VII) and the ability to incorporate Tc(IV) within the fibers. It is also worth noting that the observed enhancement of crystallinity of the composite matrix upon reductive TcO$_4^-$ uptake as seen in the TEM analyses points to a structural reorganization or phase transformation process. This transformation of the polycrystalline matrix leading to the dominance of the cassiterite phase is not observed when the control composite is exposed to DI water alone but only when it is treated with an aqueous solution of TcO$_4^-$. This transformation triggered by the incorporation of Tc is presumably suggestive of the cassiterite recognition of Tc(IV). It has been shown previously that TcO$_2$ can adapt a rutile structure.[18] While the ionic radius of octahedral Tc(IV) (78.5 pm) is slightly lower than octahedral Sn(IV) (83 pm),[38] the highly polarizable nature of Tc(IV) makes it a likely candidate for structural incorporation within frameworks of moderately different sizes.[39] As a representative example, while similar differences exist between the ionic radii of Tc(IV) and Ti(IV) (74.5 ppm), the feasibility of Tc(IV) incorporation in the TiO$_2$
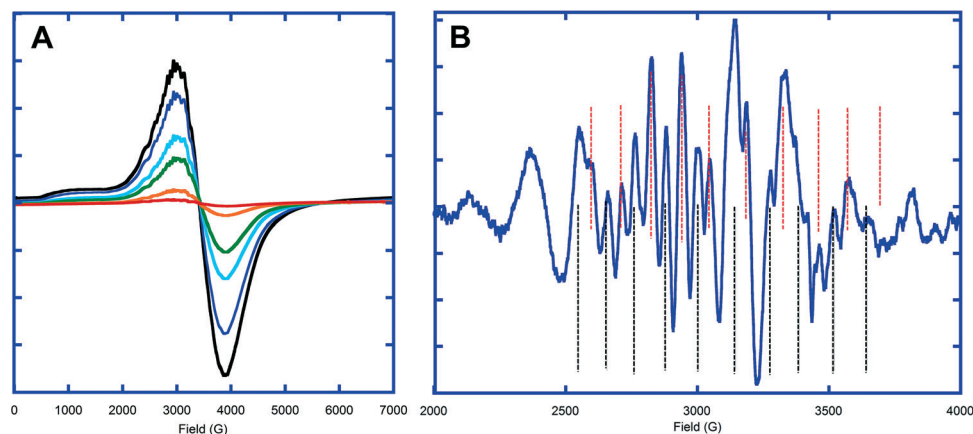
Fig. 5 (A) Temperature-dependent EPR spectra of the Tc-loaded **Sn–Al–PO$_4$** composite at 125 K (red trace), 75 K (orange trace), 35 K (green trace), 15 K (sky blue trace), 4 K (Persian blue trace), and 2.5 K (black trace). (B) Hyperfine profile extracted from the spectrum obtained at 125 K showing two different sets of 10 resonances corresponding to Tc(IV) marked in black and red dashed lines.

1010 | *Environ. Sci.: Nano*, 2016, **3**, 1003–1013

This journal is © The Royal Society of Chemistry 2016

rutile structure has been demonstrated both by theoretical calculations[19] and experimentally.[40] The detailed investigation of such a mechanism is under way and may have implications for the fabrication of these materials as low-temperature waste forms for Tc. It is worth mentioning that while such recognition has played an important role in the detection of contaminants including the detection of TcO_4^-,[41] to date its practical implementation for the reductive uptake of TcO_4^- has not been realized in part because quantitative sequestration of Tc(IV) in such structures as goethite relies on *in situ* formation of Tc-bearing goethite in the contaminated solution stream[5] and is hard to achieve in the multicomponent process systems. Application of the solid Sn–Al–PO$_4$ composite for Tc separation and sequestration can address this challenge and have implications in the selective reductive removal and long-term storage of TcO_4^- in particular and other redox active contaminants in general.

TcO_4^- uptake kinetics by Sn–Al–PO$_4$ from complex alkaline solutions

The performance of the Sn–Al–PO$_4$ composite for the Tc reductive sorption from high in ionic strength alkaline solutions was evaluated. The kinetics of the TcO_4^- uptake from 2 M NaOH/2 M NaNO$_3$ was monitored for 24 hours. The composite exhibited fast kinetics and high efficiency of uptake, approaching the equilibrium Tc K_d value of ~13 000 mL g^{-1} at 24 hours and with near-quantitative TcO_4^- uptake (98%) as shown in Fig. 6.

Subsequently, the Sn–Al–PO$_4$ composite was challenged under the LAW simulant conditions. The LAW simulant is a complex mixture of mostly sodium salts with a total Na$^+$ concentration of 7.8 M and a free OH$^-$ concentration of 2.34 M (Table 1). It contains several inorganic anions, which potentially could interfere with Tc incorporation into the composite matrix. A plot of K_d values for the composite, obtained using the LAW simulant in the absence of CrO_4^{2-}, is represented as a function of time in Fig. 6. The kinetics of the uptake appeared to be slightly slower in LAW simulant than in the 2 M NaOH/2 M NaNO$_3$ solution. Remarkably, the equilibrium K_d value observed in the LAW simulant (~13 000 mL g^{-1}) is very similar to that in the 2 M NaOH/2 M NaNO$_3$ solution. At equilibrium, 97% of TcO_4^- was removed from the simulant. This uptake efficiency exhibited by the Sn–Al–PO$_4$ composite far exceeds that of Sn(II)-based hydroxyapatite or Sn(II)-based apatite composites that have been conventionally recommended for TcO_4^- uptake under these LAW simulant conditions, which are representative of tank LAWs.[22] The observed K_d value is comparable to that shown by potassium metal sulphide (KMS), whose high K_d is attributed to the effectiveness of the sulfide reduction of Tc(VII) to Tc(IV).[42] It should be noted that in the literature experiments the simulant-to-sorbent ratio of 100 mL g^{-1} was employed compared to the much more challenging ratio of 1000 mL g^{-1} utilized in this work.

Slower kinetics and about 6-fold reduction of the equilibrium K_d value to ~2200 mL g^{-1} are observed in the LAW simulant containing 33 mM CrO_4^{2-} (Fig. 5). At equilibrium, 68% of TcO_4^- was removed from the Cr(VI)-containing simulant. The diminished performance of the Sn–Al–PO$_4$ composite is due to the fact that the highly oxidizing CrO_4^{2-} can disrupt the redox process. Consideration of the standard redox potentials in alkaline media for TcO_4^-/TcO_2, $E_0 = -0.74$ V; Sn(OH)$_6^{2-}$/HSnO$_2^-$, $E_0 = -0.93$ V; and CrO_4^{2-}/Cr(OH)$_3$, $E_0 = -0.13$ V (ref. 43) suggests that CrO_4^{2-} can interfere with TcO_4^- reductive sorption in two ways: (i) partially oxidize the Sn(II) centre to Sn(IV) before it can react with TcO_4^- and so diminish the overall reductive capacity of the composite or (ii) partially reoxidize the generated Tc(IV) back to TcO_4^-. The observation that the LAW simulant solution changes color from yellow to green upon contact with the composite supports this hypothesis by indicating the reduction of CrO_4^{2-} to Cr(OH)$_3$. Nevertheless, the K_d value of ~2200 mL g^{-1} determined in the presence of chromate is reasonable for practical removal of TcO_4^-
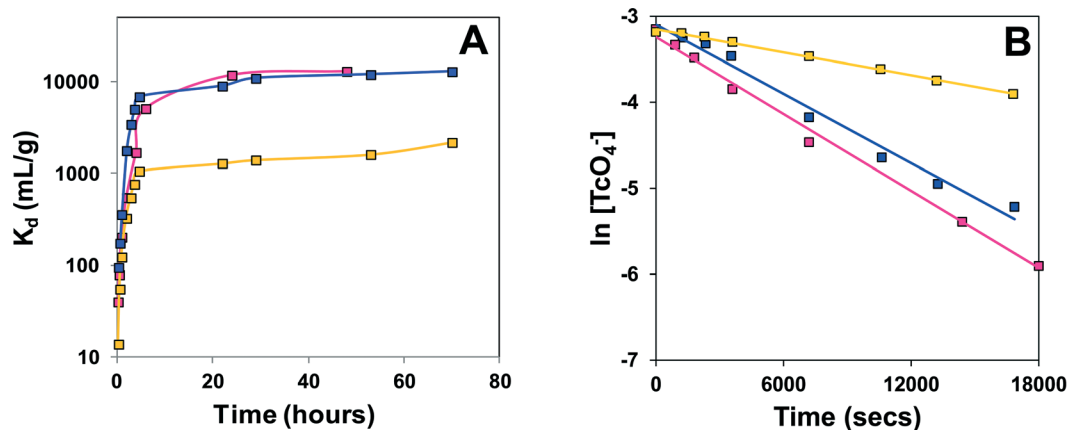
Fig. 6 (A) Kinetics of TcO_4^- removal by Sn–Al–PO$_4$ composite from 2 M NaOH/2 M NaNO$_3$ (purple line and symbols), LAW simulant in the absence of CrO_4^{2-} (blue line and symbols), and LAW simulant in the presence of CrO_4^{2-} (yellow line and symbols). (B) Corresponding semi-logarithmic plots of the TcO_4^- molar concentration in the contact solutions *vs.* time. Regression analyses for the plots: $\ln[TcO_4^-] = -1.5 \times 10^{-4} t - 3.93$, $R^2 = 0.9955$ (purple line); $\ln[TcO_4^-] = -1.34 \times 10^{-4} t - 3.10$, $R^2 = 0.9940$ (blue line); $\ln[TcO_4^-] = -4.5 \times 10^{-5}t - 3.15$, $R^2 = 0.9967$ (yellow line).

This journal is © The Royal Society of Chemistry 2016

Environ. Sci.: Nano, 2016, **3**, 1003–1013 | **1011**

from tank supernatants containing Cr(VI). The overall observation validates our initial hypothesis that the selectivity of the Sn-based composites can be significantly improved by association of the reduced Tc(IV) with the composite structure.

Fig. 6B shows that the concentration of TcO_4^- in the contact solutions can be fit to a logarithmic behaviour with respect to time, suggesting a first-order process for TcO_4^- sorption. The first-order kinetic rate constant, obtained from the plot's slope for the sorption of Tc from the LAW simulant performed in the absence of CrO_4^{2-} is -1.34×10^{-4} s^{-1} which is comparable to that obtained using the 2 M NaOH/2 M NaNO$_3$ matrix (-1.5×10^{-4} s^{-1}). As with the lowering of the K_d value upon the inclusion of CrO_4^{2-} in the LAW simulant, a similar reduction is observed in the slope as well, with the value of the slope obtained in the presence of chromate being -4.5×10^{-5} s^{-1}. Again, this slower uptake kinetics is presumably due to the competing reduction of Cr(VI).

It should be noted that neither decomposition nor dissolution of the Sn–Al–PO$_4$ composite in the LAW simulant with or without the presence of Cr(VI) was observed within 72 hours of the batch contact experiment.

Summary

The diffraction and microscopy studies presented here illustrate that the **Sn–Al–PO$_4$** composite obtained by a simple hydrothermal synthesis consists of structurally well-defined Sn(II/IV)-rich fibers dispersed within a heterogeneous Sn–Al–PO$_4$ matrix. The composite consists of several crystalline and polycrystalline phases that prove to be beneficial for the reductive separation of TcO_4^-. The composite's effectiveness in removal of TcO_4^- is promoted by the Sn-rich fibers facilitating the reduction of TcO_4^- to Tc(IV) as supported by the XPS measurements and Tc(IV) subsequent deposition along the fiber branches. A cassiterite, SnO$_2$ with rutile structure is formed within the polycrystalline matrix, and our results are consistent with Tc(IV) incorporation into this phase. The Tc(IV) embedded within the **Sn–Al–PO$_4$** matrix demonstrates high resistance to oxidation to TcO_4^- as evidenced by the XPS of the Tc-loaded composite after 6 months of loading showing preservation of Tc(IV) and no formation of Tc(VII). This result is in unison with the observation that the **Sn–Al–PO$_4$** composite exhibits a high K_d value for Tc even in the presence of the strong oxidant CrO_4^{2-}. This warrants future studies of electroanalytical determination of redox potentials for the Tc(IV) loaded **Sn–Al–PO$_4$** matrix and how they compare with pure Tc(IV) species.

The **Sn–Al–PO$_4$** composite is highly efficient for removing TcO_4^- not only from simple caustic matrices (2 M NaOH/2 M NaNO$_3$) but also from complex LAW simulants and appears to be suitable for practical reductive separation of TcO_4^- from tank waste streams. Significantly, this material offers improved selectivity over Cr(VI) over previously studied pertechnetate getters. Moreover, the uptake/removal is highly specific for TcO_4^- even in the presence of other interfering anions as illustrated by the high removal from LAW simulant containing Cl$^-$, CO$_3^{2-}$, NO$_2^-$, NO$_3^-$, PO$_4^{3-}$, SO$_4^{2-}$ and OH$^-$ at concentrations significantly greater than that of TcO_4^-. Future studies are warranted to evaluate the utility of the Sn–Al–PO$_4$ composite to improve the performance of cementitious waste forms with respect to their oxidative stability and ability to inhibit leaching of Tc(IV) incorporated into the composite matrix.[44]

Acknowledgements

References

1 R. E. Wildung, K. M. Mcfadden and T. R. Garland, *J. Environ. Qual.*, 1979, **8**, 156.

2 ICRP, *Radionuclide Transformations – Energy and Intensity of Emissions*, ICRP Publication 38, Ann. ICRP 11–13, 1983.

3 R. E. Wildung, T. R. Garland, K. M. Mcfadden and C. E. Cowan, *Technetium sorption in surface soils*, Elsevier, London, 1986.

4 J. G. Darab, A. B. Amonette, D. S. D. Burke, R. D. Orr, S. M. Ponder, B. Schrick, T. E. Mallouk, W. W. Lukens, D. L. Caulder and D. K. Shuh, *Chem. Mater.*, 2007, **19**, 5703.

5 W. Um, H. S. Chang, J. P. Icenhower, W. W. Lukens, R. J. Serne, N. P. Qafoku, J. H. Westsik, E. C. Buck and S. C. Smith, *Environ. Sci. Technol.*, 2011, **45**, 4904.

6 T. A. Marshall, K. Morris, G. T. W. Law, J. F. W. Mosselmans, P. Bots, S. A. Parry and S. Shaw, *Environ. Sci. Technol.*, 2014, **48**, 11853.

7 T. Peretyazhko, J. M. Zachara, S. M. Heald, B. H. Jeon, R. K. Kukkadapu, C. Liu, D. Moore and C. T. Resch, *Geochim. Cosmochim. Acta*, 2008, **72**, 1521.

8 Y. Liu, J. Terry and S. Jurisson, *Radiochim. Acta*, 2008, **96**, 823.

9 J. H. P. Watson and D. C. Ellwood, *Nucl. Eng. Des.*, 2003, **226**, 375.

10 W. Eckelman and P. Richards, *J. Nucl. Med.*, 1970, **11**, 761.

11 P. Warwick, S. Aldridge, N. Evans and S. Vines, *Radiochim. Acta*, 2007, **95**, 709.

12 E. Yalcintas, X. Gaona, A. C. Scheinost, T. Kobayashi, M. Altmaier and H. Geckeis, *Radiochim. Acta*, 2015, **103**, 57.

13 J. B. Duncan, K. Hagerty, W. P. Moore, R. N. Rhodes, J. M. Johnson and R. C. Moore, *Laboratory Report On The Reduction And Stabilization (Immobilization) Of Pertechnetate To Technetium Dioxide Using Tin(II) apatite*, Report Number: LAB-RPT-12-00001 Revision 0, Washington River Protection Solutions, LLC, Washington, 2012.

14 R. M. Asmussen, J. J. Neeway, A. R. Lawter, W. W. Lukens and N. P. Qafoku, in *Waste Management Conference*, Phoenix, AZ, 2015, vol. Paper 15420.

15 D. M. Wellman, S. V. Mattigod, K. E. Parker, S. M. Heald, C. M. Wang and G. E. Fryxell, *Inorg. Chem.*, 2006, **45**, 3826.

16 W. W. Lukens, J. J. Bucher, D. K. Shuh and N. M. Edelstein, *Environ. Sci. Technol.*, 2005, **39**, 8064.

17 J. K. Fredrickson, J. M. Zachara, A. E. Plymale, S. M. Heald, J. P. McKinley, D. W. Kennedy, C. X. Liu and P. Nachimuthu, *Geochim. Cosmochim. Acta*, 2009, **73**, 2299.

18 E. E. Rodriguez, F. Poineau, A. Llobet, A. P. Sattelberger, J. Bhattacharjee, U. V. Waghmare, T. Hartmann and A. K. Cheetham, *J. Am. Chem. Soc.*, 2007, **129**, 10244.

19 E. Y. Kuo, M. J. Qin, G. J. Thorogood, K. R. Whittle, G. R. Lumpkin and S. C. Middleburgh, *J. Nucl. Mater.*, 2013, **441**, 380.

20 M. Sanchez-Sanchez, R. van Grieken, D. P. Serrano and J. A. Melero, *J. Mater. Chem.*, 2009, **19**, 6833.

21 P. J. Certa, P. A. Empey and M. N. Wells, *River Protection Project System Plan*, Report Number: ORP-11242, Revision 6, Washington River Protection Solutions, LLC, Washington, 2011.

22 N. Qafoku, J. J. Neeway, A. R. Lawter, T. G. Levitskaia, R. J. Serne, J. J. H. Westsik and M. M. V. Snyder, *Technetium and Iodine Getters to Improve Cast Stone Performance*, Report Number: PNNL-23282, Pacific Northwest National Laboratory, Washington, 2014.

23 S. F. Weng, K. B. Chen and C. S. Lee, *Solid State Sci.*, 2008, **10**, 1485.

24 A. Dutta, D. Gupta, A. K. Patra, B. Saha and A. Bhaumik, *ChemSusChem*, 2014, **7**, 925.

25 N. K. Mal, S. Ichikawa and M. Fujiwara, *Chem. Commun.*, 2002, 112.

26 M. Wei, X. Y. Xu, X. R. Wang, F. Li, H. Zhang, Y. L. Lu, M. Pu, D. G. Evans and X. Duan, *Eur. J. Inorg. Chem.*, 2006, 2831.

27 W. Y. Huang, S. Komarneni, A. R. Aref, Y. D. Noh, J. F. Ma, K. F. Chen, D. F. Xue and B. B. Jiang, *Chem. Commun.*, 2015, **51**, 15661.

28 K. Utchariyajit and S. Wongkasemjit, *Microporous Mesoporous Mater.*, 2008, **114**, 175.

29 D. L. Sun, J. R. Deng and Z. S. Chao, *Chem. Cent. J.*, 2007, **1**, 27.

30 *Powder Diffraction File Inorganic and Organic Data Book*, ed. S. Kabekkodu, International Center for Diffraction Data, Newtown Square, PA, USA, 2015, vol. 60.

31 X. Y. Hou, Y. J. Hu, H. Jiang, Y. F. Li, W. G. Li and C. Z. Li, *J. Mater. Chem. A*, 2015, **3**, 9982.

32 H. K. Wang, K. P. Dou, W. Y. Teoh, Y. W. Zhan, T. F. Hung, F. H. Zhang, J. Q. Xu, R. Q. Zhang and A. L. Rogach, *Adv. Funct. Mater.*, 2013, **23**, 4847.

33 M. Thompson, A. D. Nunn and E. N. Treher, *Anal. Chem.*, 1986, **58**, 3100.

34 D. W. Wester, D. H. White, F. W. Miller, R. T. Dean, J. A. Schreifels and J. E. Hunt, *Inorg. Chim. Acta*, 1987, **131**, 163.

35 G. Romelt and K. Schwocha, *Z. Naturforsch., A: Astrophys., Phys. Phys. Chem.*, 1967, **22**, 519.

36 H. H. Pieper and K. Schwochau, *J. Chem. Phys.*, 1975, **63**, 4716.

37 W. W. Lukens, J. J. Bucher, N. M. Edelstein and D. K. Shuh, *Environ. Sci. Technol.*, 2002, **36**, 1124.

38 R. D. Shannon, *Acta Crystallogr., Sect. A: Cryst. Phys., Diffr., Theor. Gen. Crystallogr.*, 1976, **32**, 751.

39 F. N. Skomurski, K. M. Rosso, K. M. Krupka and B. P. McGrail, *Environ. Sci. Technol.*, 2010, **44**, 5855.

40 N. P. Laverov, S. V. Yudintsev and B. I. Omel'yanenko, *Geol. Ore Deposits*, 2009, **51**, 259.

41 S. Chatterjee, A. E. Norton, M. K. Edwards, J. M. Peterson, S. D. Taylor, S. A. Bryan, A. Andersen, N. Govind, T. E. Albrecht-Schmitt, W. B. Connick and T. G. Levitskaia, *Inorg. Chem.*, 2015, **54**, 9914.

42 J. J. Neeway, R. M. Asmussen, A. R. Lawter, M. E. Bowden, W. W. Lukens, D. Sarma, B. J. Riley, M. G. Kanatzidis and N. P. Qafoku, *Chem. Mater.*, 2016, **28**, 3976.

43 A. J. Bard, R. Parsons and J. Jordan, *Standard Potentials in Aqueous Solutions*, IUPAC (Marcel Dekker), New York, USA, 1985.

44 J. Westsik Jr, K. J. Cantrell, R. J. Serne and N. Qafoku, *Technetium Immobilization Forms Literature Survey*, Pacific Northwest National Laboratory, 2014.